Theoretical Analysis of Gas-Phase Front-Side Attack Identity $S_N2(C)$ and $S_N2(Si)$ Reactions with Retention of Configuration

Zhong-Zhi Yang,* Yan-Li Ding, and Dong-Xia Zhao

Chemistry and Chemical Engineering Faculty, Liaoning Normal University, Dalian 116029, P. R. China

Received: May 22, 2008; Revised Manuscript Received: December 24, 2008

Gas-phase front-side attack identity $S_N2(C)$ and $S_N2(Si)$ reactions, $CH_3X1 + X2^- \rightarrow CH_3X2 + X1^-$ and $SiH_3X1 + X2^- \rightarrow SiH_3X2 + X1^-$ (X = F, Cl), are investigated by the ab initio method and molecular face (MF) theory. The computations have been performed at the CCSD(T)/aug-cc-pVTZ//MP2/6-311++G(3df,3pd) and CISD/aug-cc-pVDZ levels. Front-side attack identity S_N2 reactions for both SiH_3X and CH_3X have double-well potential energy surfaces (PESs), but their transition-state positions are different relative to the positions of reactants and products: it is lower for SiH_3X, and it is higher for CH_3X. The minimum energy path for an $S_N2(Si)$ reaction with retention of configuration proceeds from a stable pentacoordinated anion intermediate of C_s symmetry (TBP) via a C_s transition state (SP) to a complementary pentacoordinated intermediate (TBP) and finally up to separate products. Berry pseudorotation has been observed in the front-side attack identity $S_N2(Si)$ reactions with F^- and Cl^- along the intrinsic reaction coordinate (IRC) routes. In addition, the geometrical transformations of front-side attack identity $S_N2(C)$ and $S_N2(Si)$ reactions based on the IRC calculations at the MP2/6-311++G(3df, 3pd) level of theory are described compared with those of corresponding back-side attack reactions. The difference between front-side attack identity $S_N2(C)$ and $S_N2(Si)$ reactions has been demonstrated. In MF theory, the potential acting on an electron in a molecule (PAEM) is an important quantity; in particular, its D_{pb} can measure the strength of a chemical bond in a molecule. It is found that the difference between D_{pb} values of reactant and transition state may be related to the activation energy for front-side and back-side attack $S_N2(C)$ and $S_N2(Si)$ reactions, and the D_{pb} curves along the IRC routes have features similar to those of the potential energy profiles for all of the back-side attack S_N2 reactions and front-side attack $S_N2(Si)$ reaction with F^-. Furthermore, according to the MF theory, the spatial dynamic changing features of the molecular shapes and the face electron density are vividly depicted for the course of the reactions.

1. Introduction

Bimolecular nucleophilic substitution reaction at carbon ($S_N2(C)$) is one of the most elementary chemical reactions that plays an important role in organic and biological chemistry.[1−13] Various experimental and theoretical studies have focused on back-side attack $S_N2(C)$ reactions with inversion of configuration,[3−7] which is the preferred stereochemical route in gas phase. In contrast, front-side attack $S_N2(C)$ reactions with retention of configuration have been less investigated. Previous studies[8−13] have shown that a front-side attack $S_N2(C)$ reaction with retention of configuration proceeds at higher energies, and the retention mechanism differs from the traditional back-side S_N2 route. For a front-side attack $S_N2(C)$ reaction, initially, an ion−molecule complex of C_{3v} symmetry is formed with a complexation energy, E_{comp}. (Refer to Scheme 1a.) Then, it must overcome an activation barrier, that is, $E^{\#}_{cent}$, to reach the transition state of C_s symmetry. Afterward, the state goes down to the post-ion−molecule complex that is equivalent to the pre-ion−molecule complex. Finally, it dissociates into separate products. Here we have undertaken a high-level computational study for an anion for the identity S_N2 reactions

$$CH_3X1 + X2^- \rightarrow CH_3X2 + X1^- (X = F, Cl) \qquad (1)$$

The S_N2 reactions at silicon ($S_N2(Si)$) have been investigated in both experimental work[14−19] and theoretical calculations.[20−26] For an $S_N2(Si)$ reaction with retention of configuration, previous studies have proposed two possible retention mechanisms. The first one, illustrated in Scheme 2a, is the same mechanism as that for the retention mechanism in nucleophilic substitution reactions of phosphorus.[27,28] It involves axial entry and axial departure accompanied by Berry pseudorotation[29] of the initially formed five-coordinate activated state. The pseudorotation proceeds by the initial trigonal bipyramid (TBP) passing through a square pyramid (SP) to a rearranged TBP. The X-ray results have shown that anionic five-coordinated silicon derivatives are nonrigid and display progressive distortions between the TBP and SP.[14−18] The second one, an alternative retention mechanism (Scheme 2b) proposed by Corriu,[30] does not require a pseudorotation step. In our study, it is found that the $S_N2(Si)$ reactions with retention of configuration also have a double-well potential energy surface (PES). The reactants initially form a stable pentacoordinated anion intermediate of C_s symmetry (Scheme 2a′, TBP) and then proceed through a C_s transition state (Scheme 2a′, SP) to a rearranged pentacoordinated anion intermediate (Scheme 2a′, TBP) and finally dissociate into separate products. Importantly, these reactions proceed via Berry pseudorotation. Here two reactions with retention of configuration have been investigated

$$SiH_3X1 + X2^- \rightarrow SiH_3X2 + X1^- (X = F, Cl) \qquad (2)$$

The schematic energy profile of the reactions is shown in Scheme 1b.

* Corresponding author. E-mail: zzyang@lnnu.edu.cn.

10.1021/jp804951w CCC: $40.75
Published on Web 04/08/2009

SCHEME 1: Schematic Energy Profiles for the Identity Exchange Reactions $CH_3X1 + X2^- \rightarrow CH_3X2 + X1^-$ and $SiH_3X1 + X2^- \rightarrow SiH_3X2 + X1^-$ (X = F, Cl) with Retention and Inversion of Configuration along the IRC Routes

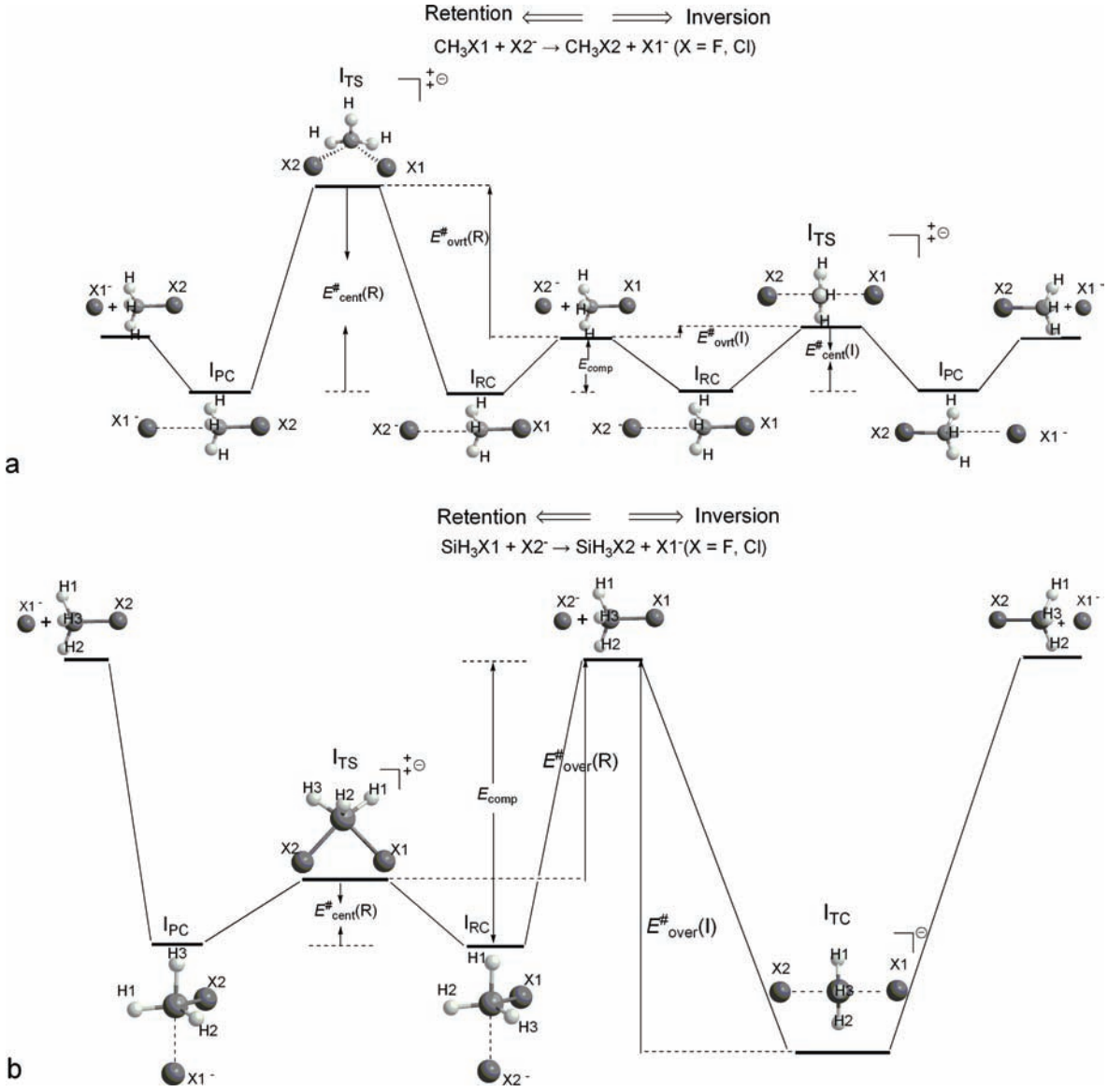

In this work, $S_N2(C)$ and $S_N2(Si)$ reactions with retention of configuration have been systemically investigated at the CCSD(T)/aug-cc-pVTZ//MP2/6-311++G(3df,3pd) and CISD/aug-cc-pVDZ levels of theory. The results have been compared with those of the corresponding back-side attack reactions with inversion of configuration. The four types of attacks of an anion X^- have been analyzed for retention and inversion pathways. The geometries of stationary points, intrinsic reaction coordinate (IRC) calculations, potential energy profiles, and possibility of retention pathway have been discussed in detail and compared with the inversion pathway. The difference between gas-phase $S_N2(C)$ and $S_N2(Si)$ reactions with retention of configuration has been demonstrated. In particular, in our studies, the Berry pseudorotation[29] of the gas-phase front-side attack identity $S_N2(Si)$ reactions has been observed. Furthermore, we present a theoretical analysis of the $S_N2(C)$ and $S_N2(Si)$ reactions by the molecular face (MF) theory. An MF represents both its molecular shape and its face electron density,[31−40] which is a new model. Yang and coworkers have explored the shape-changing pictures during the process of forming H_2 from two separate hydrogen atoms by the MF theory.[33] Recently, the interesting polarization and bonding interaction pictures between a hydrogen atom and a fluorine atom[34] as well as an organic chemical reaction[37] about $F + C_2H_2$ have been investigated by means of the MF theory. Very recently, the Markovnikov reactions of alkenes have been well studied by MF theory.[39]

This article is organized as follows: In the next section, we briefly describe the theoretical basis used in this article. Section 3 contains the ab initio study on S_N2 reactions, the difference between reactions 1 and 2, the studies on S_N2 reactions by D_{pb}, and the dynamic changing features of the MF. The last section gives a brief conclusion.

2. Theory

2.1. Ab Initio Method. From the previous very large number of calculations already carried out on S_N2 reactions, it is clear that the computational data are sensitive to the level of theory employed. Therefore, to improve the accuracy, the CCSD(T)[41] method with aug-cc-pVTZ[42] basis set was used to calculate the single-point energies with zero-point vibrational energy (ZPE) on the basis of the MP2[43]/6-311++G(3df, 3pd)[44] geometries. In this work, all stationary points were characterized by harmonic vibration analyses employing energy Hessians. IRC[45]

SCHEME 2: (a) Mechanism 1 for S_N2(Si) Reactions with Retention of Configuration via Berry Pseudorotation, (a′) Scheme of the Mechanism 1 for the Reactions $SiH_3X1 + X2^- \rightarrow SiH_3X2 + X1^-$ (X = F, Cl) with Retention of Configuration Via Berry Pseudorotation, and (b) Mechanism 2 for the S_N2(Si) Reactions with Retention of Configuration

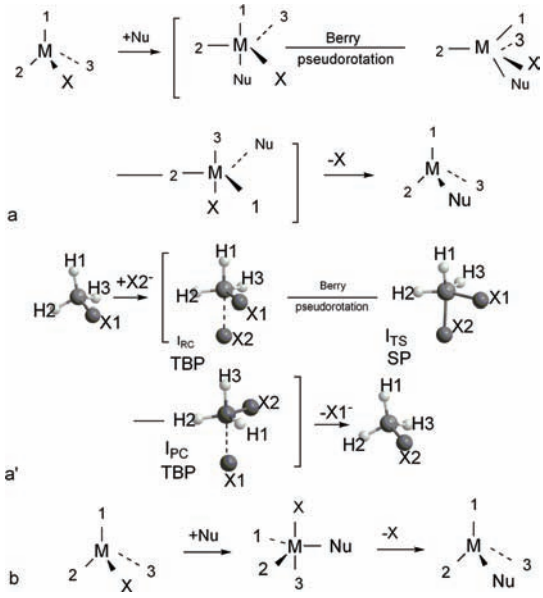

calculations were performed with the Gaussian 03 program at the MP2/6-311++G(3df, 3pd) level of theory.

2.2. Potential Acting on an Electron in a Molecule and Molecule Face. The potential acting on an electron in a molecule (PAEM) is defined as the interaction energy of a local electron that belongs to a molecule with the rest of the particles of the molecule, namely, all of the nuclei and the remaining electrons. In the molecular electronic ground state, the PAEM can be expressed as[31−40]

$$V(r) = -\sum_{A} \frac{Z_A}{r_A} + \frac{1}{\rho(r)} \int \frac{\rho_2(r, r')}{|r - r'|} \, dr' \qquad (3)$$

in which the first term is the attractive potential provided by all of the nuclei and the second term is the Coulomb interaction potential of the considered electron with the remaining electrons of the molecule. Z_A is the charge on nucleus A, r_A stands for the distance of nucleus A to the electron considered, summation involving index A is over all the nuclei, r and r' denote the electronic coordinates, $\rho(r)$ is the one-electron density function of finding an electron at r, and $\rho_2(r,r')$ is the two-electron density function of finding an electron at r and at the same time another electron at r'. In the configuration interaction (CI) method, $\rho(r)$ and $\rho_2(r,r')$ can be specifically expressed as a combination of molecular integrals obtained by an ab initio method. The PAEM is essentially different from the molecular electrostatic potential (MEP), as discussed in detail in ref 38.

Let us see an electron that moves in a molecule. When its energy is equal to its felt potential (i.e., the PAEM), this position R is a classical turning point of this electron movement. Assuming that the one-electron energy at R is equal to the minus of the first ionization potential of the molecule,[31−40] we have the formula, $V(R) = -I$, that is, the classical turning point equation of this electron movement, and where $V(R)$ is the PAEM defined by eq 3 and I is the first ionization potential of the molecule, this point R is called a molecular intrinsic characteristic point. Collecting all of these points and depicting a surface passing through them defines a molecular intrinsic characteristic contour (MICC). The electron density value on each MICC point can also be calculated, so a MICC with electron density (MICCED) can be constructed. The MICCED is an intrinsic characteristic "face" or "fingerprint" for a molecular system and is called a molecular face (MF). The MF has a clear physical meaning because it is composed of all of the classical turning points of electron movement in the molecule.

The PAEM was calculated by the CI method with all single and double substitutions (CISD) in conjunction with the aug-cc-pVDZ basis set. The calculations were performed using the ab initio MELD[46] program and a separate code developed by us. In this article, vertical ionization potentials for the structures considered were adopted and calculated at the CCSD(T)/aug-cc-pVTZ level of theory using the Gaussian 03 program. Drawing a 3D characteristic contour with encoded electron density as 4D (i.e., MF) was done by means of Matlab 7.0 software.

3. Results and Discussion

3.1. Ab Initio Study on S_N2(C) and S_N2(Si) Reactions with Retention of Configuration. ***3.1.1. Analysis of Retention and Inversion Pathways.*** *Pathway Geometries.* The pathway geometries of S_N2(C) and S_N2(Si) reactions were optimized at the MP2/6-311++G(3df, 3pd) level of theory. For these reactions, there are usually four types of attacks, that is, an anion X^- attacks at the H−H−H face, the H−H−X face, the H−H edge, and the H−X edge of CH_3X or SiH_3X (X = F, Cl), respectively. The H−H−H face attack leads an S_N2 reaction to proceed via the back-side attack pathway, whereas the other three attacks lead an S_N2 reaction to proceed via the front-attack pathway. These four types of attacks can be studied by geometry "optimizations" which are performed by constraining the distances between the central atom and nucleophile at different values (3.950, 3.500, 3.000, 2.500, and 2.000 Å) and by constraining the attack orientation. The calculated geometries are given in the Supporting Information (Tables S1−S4).

Total Energies. Total energies were calculated at the CCSD(T)/aug-cc-pVTZ level of theory on the basis of the above "optimized " geometries. The calculated energy values are listed in Table 1. Some features can be abstracted from the results of the energy calculations. For the S_N2(C) reactions with F^- and Cl^-, the H−H−H face attacks are the lowest in energy, so the back-side attack pathways are relatively easy. Interestingly, the H−H edge attacks are lower in energy than the H−H−X face and H−X (X = F, Cl) edge attacks, indicating that S_N2(C) reactions with retention of configuration proceed via the route in which the nucleophile attacks the H−H edge. It has been justified by following IRC calculation and analysis in Section 3.1.2. Note that the H−H−X face attack is lower in energy than the H−H edge attack, where the distance between the central atom and nucleophile is less than 2.500 Å, whereas the pre-ion−molecule complex, which is equivalent to that of the back-side attack reaction, is formed before a distance of 2.500 Å (3.318 Å for reaction with Cl^- and 2.584 Å for reaction with F^-). For the S_N2(Si) reactions with F^- and Cl^-, the H−H−H face attacks are the lowest in energy, then the H−H−X face attacks, next the H−H edge attacks, and lastly the H−X edge attacks. This is consistent with the following studies of IRC routes. A back-side attack S_N2(Si) reaction proceeds through initial approach of X^- (F^- or Cl^-) to the H−H−H face, whereas a front-side attack S_N2(Si) reaction prefers to attract a nucleo-

TABLE 1: Total Energies (Hartree) Obtained at the CCSD(T)/aug-cc-pVTZ Level of Theory for the S_N2(C) and S_N2(Si) Reactions

	total energy					
d[a]	∞	3.950	3.500	3.000	2.500	2.000
			$CH_3Cl + Cl^-$			
H−H−H face[b]	−959.341841	−959.353854	−959.357752	−959.358533	−959.346011	−959.354647
H−H−Cl face[c]	−959.341841	−959.321844	−959.322962	−959.320670	−959.300873	−959.220130
H−H edge[d]	−959.341841	−959.331618	−959.334096	−959.333201	−959.310112	−959.209717
H−Cl edge[e]	−959.341841	−959.317711	−959.312031	−959.285157	−959.195064	−959.215367
			$CH_3F + F^-$			
H−H−H face[b]	−239.280802	−239.292610	−239.295999	−239.300532	−239.302726	−239.288892
H−H−F face[c]	−239.280802	−239.233868	−239.235296	−239.237599	−239.239324	−239.230855
H−H edge[d]	−239.280802	−239.244835	−239.248719	−239.253853	−239.255862	−239.228264
H−F edge[e]	−239.280802	−239.231064	−239.231765	−239.231210	−239.219026	−239.146502
			$SiH_3Cl + Cl^-$			
H−H−H face[b]	−1210.412964	−1210.429621	−1210.435777	−1210.444617	−1210.453861	−1210.437440
H−H−Cl face[c]	−1210.412964	−1210.407626	−1210.414345	−1210.424340	−1210.430920	−1210.394865
H−H edge[d]	−1210.412964	−1210.406925	−1210.410847	−1210.410833	−1210.389545	−1210.291204
H−Cl edge[e]	−1210.412964	−1210.394873	−1210.390479	−1210.366815	−1210.307150	−1210.286502
			$SiH_3F + F^-$			
H−H−H face[b]	−490.375659	−490.389754	−490.395693	−490.406540	−490.424975	−490.453488
H−H−F face[c]	−490.375659	−490.349859	−490.358111	−490.373810	−490.400512	−490.439569
H−H edge[d]	−490.375659	−490.344322	−490.349716	−490.358102	−490.366345	−490.357465
H−F edge[e]	−490.375659	−490.334875	−490.338202	−490.342679	−490.341811	−490.313572

[a] d denotes distance between central atom and nucleophile. [b] Nucleophile attacks on H−H−H face, reaction proceeds via inversion pathway. [c] Nucleophile attacks on H−H−X face (X = F, Cl), reaction proceeds via retention pathway. [d] Nucleophile attacks on H−H edge, reaction proceeds via retention pathway. [e] Nucleophile attacks on H−X edge(X = F, Cl), reaction proceeds via retention pathway.

philic attack at the H−H−X face and proceeds via axial entry and axial departure.

Comparison between S_N2(C) and S_N2(Si) Reactions. With regard to the relative stabilization of the retention and inversion pathways for the reactions with the C or Si central atoms and F^- or Cl^- nucleophiles, Figure 1 gives features of the relative energies of the above-discussed points along different distances between central atom and nucleophile. Several observations can be obtained. First, for the S_N2(C) reactions, the H−H−H face attack with F^- is the lowest in relative energy (Figure 1a), followed by H−H−H face attack with Cl^-, and they both correspond to back-side attack pathways. The H−H edge attack with Cl^- is lower in relative energy before a distance of 2.500 Å than that with F^-. The H−H−Cl face and H−Cl edge attacks and the H−H−F face and H−F edge attacks are higher in relative energies than the H−H−H face and H−H edge attacks for the S_N2(C) reactions with Cl^- and F^-, respectively. Furthermore, the H−H−F face attacks are higher in relative energy than the H−H−Cl face attack before a distance of 2.500 Å. Second, for the S_N2(Si) reactions, the H−H−H face attacks with F^- and Cl^- are lower in relative energy than the other face attack and edge attacks (Figure 1b), indicating that back-side attack pathways proceed more easily compared with the other pathways. For front-side attack pathways of the S_N2(Si) reactions, the H−H−Cl face attack is lower in relative energy than the H−H−F face attack before a distance of 2.500 Å. The H−H, H−Cl, and H−F edge attacks are higher in relative energy than the face attacks. In the end, comparing S_N2(C) reactions with S_N2(Si) reactions (Figure 1c), H−H−H face attacks of S_N2(Si) reactions with both Cl^- and F^- are lower in relative energy than those of S_N2(C) reactions with Cl^- and F^-, respectively; the H−H−X face attacks of S_N2(Si) reactions are lower in relative energy than the H−H edge attacks of S_N2(C) reactions with Cl^- and F^-, respectively; the H−X edge attacks of the S_N2(Si) reaction are lower in relative energy than the H−X edge attacks of the S_N2(C) reaction with Cl^- and F^-, respectively. This indicates that replacing the central atom C by Si should make reactions with both retention and inversion of configuration more feasible.

3.1.2. Geometries of Stationary Points and Intrinsic Reaction Coordinate Calculations. *Reactants.* The optimized geometries of the reactants are listed in Table 2. The bond length deviations are generally less than 0.02 Å, and bond angle deviations are less than 0.7° compared with the experimental values.[47,48]

S_N2(C) Reactions. Figures 2 and 3 display the geometrical transformations for the S_N2(C) and S_N2(Si) processes with retention and inversion of configuration based on the IRC calculations at the MP2/6-311++G(3df, 3pd) level of theory, respectively. The optimized geometries of the complexes (intermediates) and TSs (TCs) for S_N2(C) and S_N2(Si) reactions are given in Tables 3 and 4. The front-side and back-side attack reactions both start at an identical minimum for the ion−molecule complex. (See Figure 2a,a′.) In the S_N2(C) process with inversion of configuration, $X2^-$ (nucleophile) moves along the C3 axis toward the carbon center (Figure 2a′−k′) until the X2−C bond forms completely and X1···C is completely ruptured. The reactions proceed via the Walden inversion process. In the front-side attack identity halogen (F or Cl) exchange reactions, $X2^-$ also initially moves along the C3 axis and then proceeds perpendicularly to the C3 axis toward one of the CH_3X1 hydrogens (Figure 2b). Following this, the $X2^-$ moves toward X1 of the methyl; meanwhile, the separation of the C−X1 bond is elongated and the separation of C-X2 is shortened until the three-center transition state is formed (Figure 2f). After overcoming an activation barrier, the separation of the C−X1 bond is further elongated and the separation of C-X2 bond is further shortened; then, the post-ion−molecule complex of C_{3v} symmetry is formed. Finally, it dissociates into separate products. Therefore, our results support the previous conclusions proposed by Glukhovtsev et al.[12]

S_N2(Si) Reactions. The S_N2(Si) reactions with inversion of configuration are generally thought to involve a D_{3h} transition complex (TC) of pentacoordinate silicon and do not undergo a

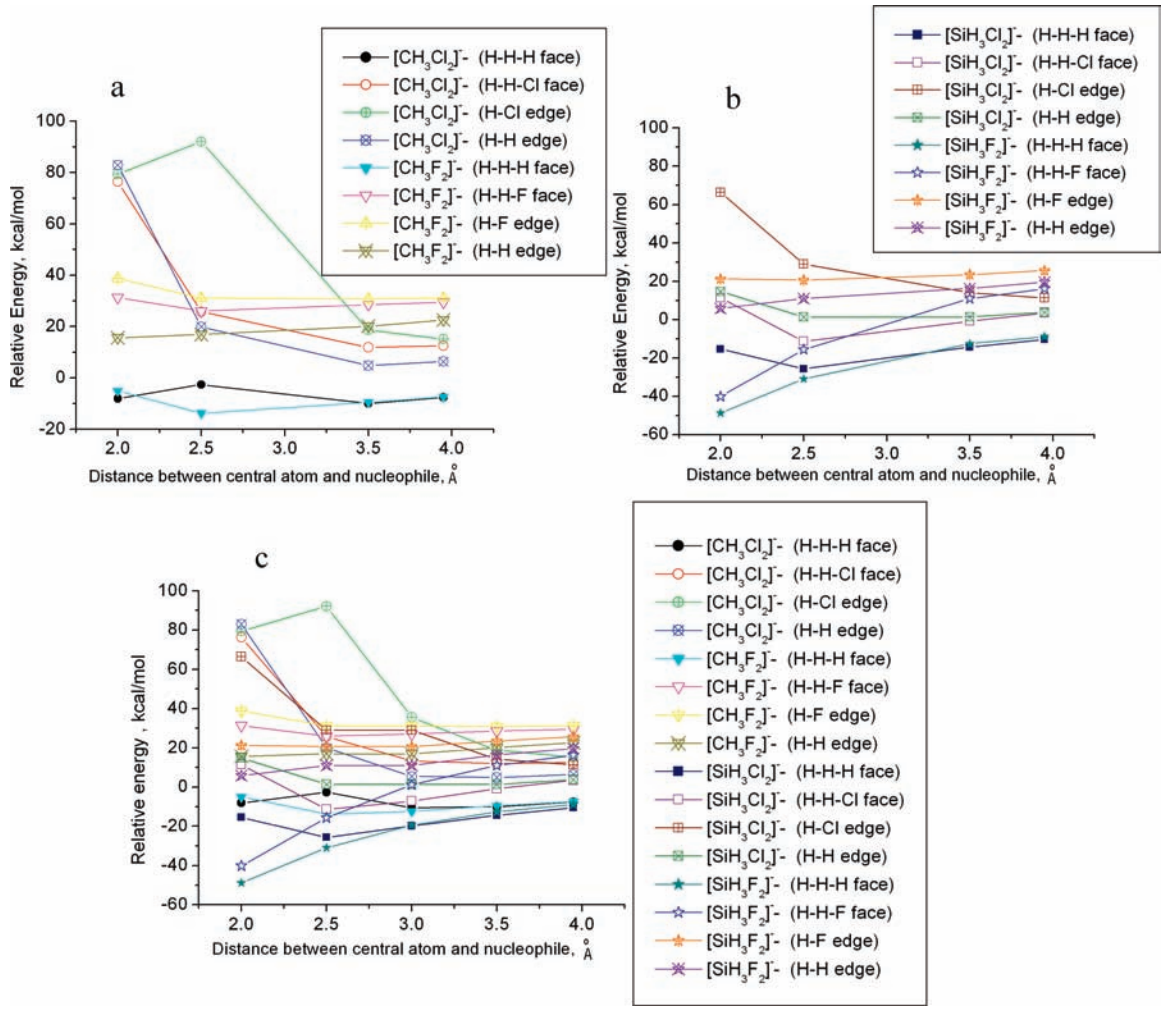

Figure 1. Curves of the relative energies obtained at the CCSD(T)/aug-cc-pVTZ level of theory based on "optimized" geometries for retention and inversion pathways.

TABLE 2: Geometries of the Reactants Calculated at the MP2/6-311++G(3df, 3pd) Level of Theory[a]

	geometry			
system	r(C−X)	r(C−H)	∠X−C−H	∠H−C−H
CH_3Cl	1.771 (1.778)[b]	1.084 (1.086)[b]	108.62 (108.2)[b]	110.31 (110.7)[b]
CH_3F	1.383 (1.382)[c]	1.086 (1.095)[c]	108.75	110.19 (110.45)[c]
system	r(Si−X)	r(Si−H)	∠X−Si−H	∠H−Si−H
SiH_3Cl	2.053 (2.048)[b]	1.468 (1.482)[b]	108.53 (107.9)[b]	110.40 (1110.0)[b]
SiH_3F	1.610 (1.593)[c]	1.468 (1.484)[c]	108.25	110.66 (110.63)[c]

[a] Experimental values in parentheses; X denotes F or Cl; bond distances in angstroms, angles in degrees. [b] Ref 47. [c] Ref 48.

pre- and post-complex (intermediate) in the course of the reactions, so only the geometries of the reactants, TCs, and products are shown in Figure 3. In the front-side attack identity halogen exchange reactions, however, $X2^-$ initially attacks the H−H−X1 (X = F, Cl) face, and then an idealized TBP, that is, a stable pentacoordinate intermediate of C_s symmetry, is formed. The separation of the Si−X1 bond is elongated, and the separation of Si−X2 is shortened until an idealized SP transition state with C_s symmetry is formed. Meanwhile, H1, H2, H3, X1, and X2 undergo a rotation. After overcoming an activation barrier, the separation of the Si−X1 bond is further elongated, and the separation of Si−X2 is further shortened, and H1, H2, H3, X1, and X2 rotate continuously. Then, a rearranged TBP forms. Finally, it dissociates into separate products (Figure 3a−i). The Berry pseudorotation of the S_N2(Si) reactions with retention of configuration has been observed along the IRC routes. In the present study, the Berry pseudorotation accompanies the changes of the bond distances and bond angles. (Refer to Table 5 and Figure 3.) Therefore, our studies further support the conclusion proposed by Holmes et al. However, Windus et al.[25] figured out that it is not generally associated with Berry pseudorotation between the pentacoordinate intermediate and TS for the $[SiH_3Cl_2]^-$ system, but it is large "precessional motion" of H and Si atoms from the study of pseudorotation of pentacoordinated silicon anion. In our studies, the Berry pseudorotation does essentially exist in the course of the front-side attack identity S_N2(Si) reactions either with Cl^- or with F^-.

Comparison between S_N2(C) and S_N2(Si) Reactions. Now we investigate the difference between front-side attack identity S_N2(C) and S_N2(Si) reactions. The main difference between them is, first, for S_N2(C) reactions, the $X2^-$ (nucleophile) initially attacks the H−H−H face that is similar to that of back-side attack ones, and then $X2^-$ proceeds perpendicularly to the C3 axis toward one of the CH_3X1 hydrogens, whereas for S_N2(Si) reactions, the $X2^-$ attacks the H−H−X1 face in the courses of the reactions. Therefore, an S_N2(C) reaction proceeds via an

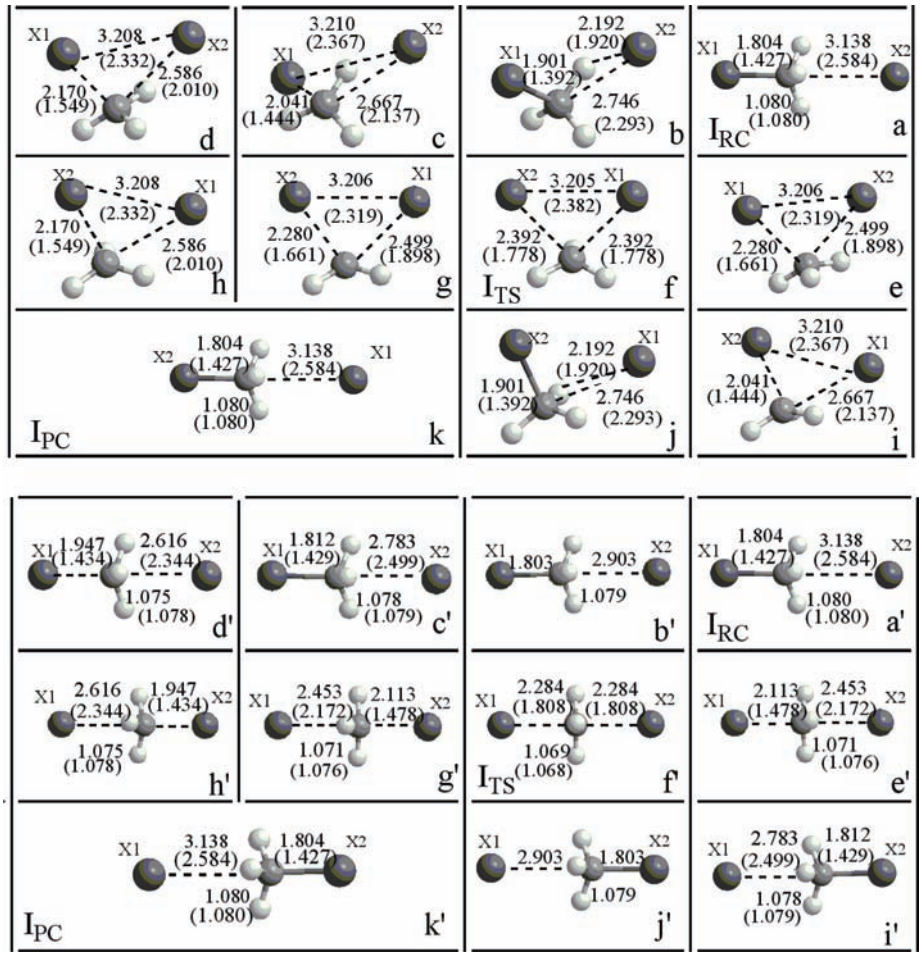

Figure 2. Atomic movements for the front-side and back-side attacks identity $S_N2(C)$ reactions with Cl^- and F^- based on the IRC calculations at the MP2/6-311++G(3df, 3pd) level of theory. X1 denotes the halogen of the neutral molecule, and X2 denotes the nucleophilic halogen. The separation between the points is 1.0 amu$^{1/2}$·bohr. The parameters of the geometries of $S_N2(C)$ reaction with F^- are given in the parentheses.

ion−molecule complex of C_{3v} symmetry, whereas an $S_N2(Si)$ reaction proceeds via a stable pentacoordinated anion intermediate of C_s symmetry (Figures 2a and 3a); second, only the reorientation appears in the course of $S_N2(C)$ reactions, whereas Berry pseudorotation essentially exists among the prepentacoordinated anion intermediate, TS, and postpentacoordinated anion intermediate along the IRC routes for front-side attack identity $S_N2(Si)$ reactions. (See Figures 2 and 3.) But they undergo similar three-center transition states, which are isoelectronic in view of valence electrons and isostructural in view of the geometric types of the main species along the IRC routes.

3.1.3. Potential Energy Profiles. The various energies calculated at the CCSD(T)/aug-cc-pVTZ level of theory are given in Table 6. The activation energies by MP2 calculations are given in the Supporting Information (Table S5), and MP2 and CCSD(T) calculated energies of reactants, complexes (intermediates), and TSs (TCs) are listed in the Supporting Information (Tables S6−S8).

Complexation Energy E_{comp}. The complexation energy is the difference in energy between the ion−molecule complex (intermediate) and the reactant, and it measures the stabilization of the former with respect to the latter. The stabilization of the ion−molecule complexes (intermediates) is in decreasing order of $[SiH_3F_2]^-$, $[CH_3F_2]^-$, $[SiH_3Cl_2]^-$, and $[CH_3Cl_2]^-$.

Central Activation Barrier $E^{\#}_{cent}$. The central activation barrier is the difference in energy between the TS and ion−molecule complex (intermediate). The central barriers of front-side attack identity $S_N2(C)$ reactions with retention of configuration are much higher than those of the corresponding back-side attack ones with inversion of configuration. (See Table 6.) The central barriers of the front-side attack identity $S_N2(Si)$ reactions are much lower than those of the $S_N2(C)$ reactions with retention and inversion of configuration, indicating that the front-side attack identity $S_N2(Si)$ reactions are much faster than the front-side attack identity $S_N2(C)$ reactions from the pre-ion−molecule (intermediate) to TS. In addition, a striking finding is that the difference between the central barriers of the $S_N2(C)$ reactions with F^- and Cl^- is small for either front-side attack reactions or back-side attack reactions (0.92 kcal mol^{-1} for the former, and 0.67 kcal mol^{-1} for the latter, respectively), but it is large for the front-side attack identity $S_N2(Si)$ reactions with F^- and Cl^- (1.76 kcal mol^{-1}).

Overall Activation Barrier $E^{\#}_{over}$. The overall activation barrier is the difference in energy between the TS and separate reactant. This barrier is decisive for the rate of chemical reaction in the gas phase. An interesting phenomenon is that the overall barriers for the front-side and back-side attacks $S_N2(Si)$ reactions are negative. (See Table 6.) The overall barriers for front-side attack identity $S_N2(C)$ reactions with Cl^- and F^- are positive, but for back-side attack reactions with Cl^- and F^-, one is positive and the other one is negative. This indicates that TSs of the $S_N2(Si)$ reactions with retention and inversion of configuration are under the separate reactants, but TSs of the front-side attack $S_N2(C)$ reactions are over the separate reactants, and for the back-side attack $S_N2(C)$ reactions, the TSs are around the separate reactants on the PESs. (See Scheme 1.) This further

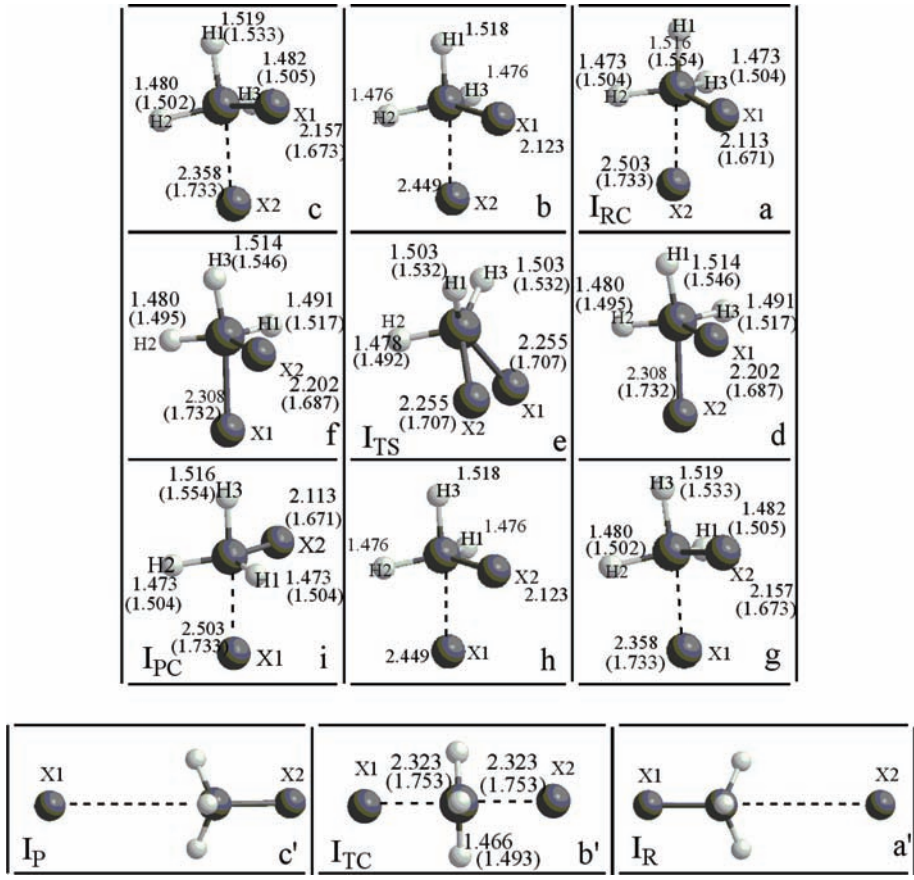

Figure 3. Atomic movements for the front-side and back-side attacks identity S_N2(Si) reactions with Cl^- and F^- based on the IRC calculations at the MP2/6-311++G(3df, 3pd) level of theory. X1 denotes the halogen of the neutral molecule, X2 denotes the nucleophilic halogen, I_R denotes reactant, and I_P denotes product. The separation between the points is 1.0 amu$^{1/2}$·bohr. The parameters of the geometries of S_N2(Si) reaction with F^- are given in the parentheses.

TABLE 3: Geometries of the Complexes (Intermediates) for the S_N2(C) and S_N2(Si) Reactions with Retention and Inversion of Configuration Calculated at the MP2/6-311++G(3df, 3pd) Level of Theory[a]

system	*r*(C−X1)	*r*(C−X2)	*r*(C−H1)	*r*(C−H2)	*r*(C−H3)	∠X1−C−X2
$[CH_3Cl_2]^-$ (R)	1.804	3.318	1.080	1.080	1.080	180.0
$[CH_3Cl_2]^-$ (I)	1.804	3.318	1.080	1.080	1.080	180.0
	(1.812)[b]	(3.148)[b]	(1.079)[b]	(1.079)[b]	(1.079)[b]	
$[CH_3F_2]^-$ (R)	1.427	2.584	1.080	1.080	1.080	180.0
$[CH_3F_2]^-$ (I)	1.427	2.584	1.080	1.080	1.080	180.0
	(1.433)[b]	(2.601)[b]	(1.079)[b]	(1.079)[b]	(1.079)[b]	
system	*r*(Si−X1)	*r*(Si−X2)	*r*(Si−H1)	*r*(Si−H2)	*r*(Si−H3)	∠X1−Si−X2
$[SiH_3Cl_2]^-$ (R)	2.113	2.503	1.516	1.473	1.473	87.98
$[SiH_3F_2]^-$ (R)	1.671	1.733	1.554	1.504	1.504	88.33

[a] R and I stand for the reactions with retention and inversion of configuration, respectively; X denotes F or Cl; bond distances in angstroms, angles in degrees. [b] Values (in parentheses) calculated at the MP2/TZ2Pf+dif level.[5]

explains that both reaction pathways of the S_N2(Si) reactions are much faster than those of the S_N2(C) reactions with F^- and Cl^-, respectively. The back-side attack identity S_N2(C) reactions are much faster than the corresponding front-side attack reactions with F^- and Cl^-, the back-side attack S_N2(Si) reaction with Cl^- is much faster than the corresponding front-side attack reaction, and the front-side attack and back-side attack S_N2(Si) reactions with F^- do not show a large difference. The change in overall barrier heights for the S_N2(C) reactions for the different halides (F and Cl) is small, but for S_N2(Si) reactions, the change is large. (See Table 6.) It shows that the rates of the front-side and back-side attack S_N2(C) reactions for F^- and Cl^- are close, whereas the front-side and back-side attack S_N2(Si) reactions with F^- are much faster than those with Cl^-.

3.1.4. Possibility for Retention Pathway with Respect to Inversion Pathway. We analyze this problem in two aspects. First, steric effect is considered. The front-side attack identity S_N2(C) and S_N2(Si) reactions might easily proceed because attacks to the backs of the CH_3X and SiH_3X (X = F, Cl) lead to steric hindrance of the three H atoms of the CH_3 and SiH_3 groups. Elongation of the bond distance between the central atom and X (X = F, Cl) would favor the retention pathway because of a reduction in the unfavorable interaction between the incoming nucleophile and leaving group. Therefore, the reactions with Cl^- favor retention of configuration compared with those with F^-. Second, electronic effect leads to favoring back-side attack pathways because Cl and F atoms of CH_3X and SiH_3X have larger negative partial charges and have strong

TABLE 4: Geometries of the TSs for the $S_N2(C)$ and $S_N2(Si)$ Reactions with Retention and Inversion of Configuration Calculated at the MP2/6-311++G(3df, 3pd) Level of Theory[a]

system	r(C−X1,2)[b]	r(C−H1)	r(C−H2,3[c])	∠X1−C−X2	∠X1−C−H1
$[CH_3Cl_2]^-$(R)	2.392	1.077	1.076	84.13	93.88
	(2.438)[d]	(1.081)[d]	(1.080)[d]	(84.2)[d]	(94.1)[d]
$[CH_3Cl_2]^-$ (I)	2.284	1.069	1.069	180.00	90.00
	(2.278)[e]	(1.067)[e]	(1.067)[e]		
$[CH_3F_2]^-$ (R)	1.778	1.081	1.097	81.14	98.55
	(1.815)[d]	(1.085)[d]	(1.099)[d]	(80.9)[d]	(98.00)[d]
$[CH_3F_2]^-$ (I)	1.808	1.068	1.068	180.00	90.00
	(1.817)[e]	(1.068)[e]	(1.068)[e]		
system	r(Si−X1,2[b])	r(Si−H1)	r(Si−H2,3[c])	∠X1−Si−X2	∠X1−Si−H1
$[SiH_3Cl_2]^-$ (R)	2.255	1.478	1.503	86.33	100.66
	(2.245)[f]	(1.484)[f]	(1.513)[f]	(89.1)[f]	(102.7)[f]
$[SiH_3Cl_2]^-$ (I)	2.323	1.466	1.466	180.00	90.00
$[SiH_3F_2]^-$ (R)	1.707	1.492	1.532	86.17	103.02
	(1.730)[f]	(1.494)[f]	(1.535)[f]	(87.2)[f]	(104.2)[f]
$[SiH_3F_2]^-$ (I)	1.753	1.493	1.493	180.00	90.00

[a] R and I stand for the reactions with retention and inversion of configuration, respectively; X denotes F or Cl; bond distances in angstroms, angles in degrees. [b] X1,2 denotes two halogen atoms X1 and X2 with the identical geometry at the TS. [c] H2,3 denotes atoms H2 and H3 with the identical geometry at TS; H1 is different hydrogen atom from atoms H2 and H3 for the S_N2 reactions with retention of configuration. [d] Values (in parentheses) calculated at the MP2/6-31+G(d) level.[12] [e] Values (in parentheses) calculated at the MP2/TZ2Pf+dif level.[5] [f] Values (in parentheses) calculated at the MP2/6-31++G(d,p) level.[25]

TABLE 5: Geometries of the Stationary Points for the Front-Side Attack Identity $S_N2(Si)$ Reactions Optimized at the MP2/6-311++G(3df, 3pd) Level of Theory[a]

system	r(Si−X1[b])	r(Si−X2[c])	r(Si−H1)	r(Si−H2)	r(Si−H3)	∠X1−Si−X2
$[SiH_3Cl_2]^-$ − I_{RC}[d]	2.113	2.503	1.516	1.473	1.473	87.98
$[SiH_3Cl_2]^-$ − I_{TS}[e]	2.255	2.255	1.503	1.478	1.503	86.33
$[SiH_3Cl_2]^-$ − I_{PC}[f]	2.503	2.113	1.473	1.473	1.516	87.98
$[SiH_3F_2]^-$ − I_{RC}[d]	1.671	1.733	1.554	1.504	1.504	88.33
$[SiH_3F_2]^-$ − I_{TS}[e]	1.707	1.707	1.532	1.492	1.532	86.17
$[SiH_3F_2]^-$ − I_{PC}[f]	1.733	1.671	1.504	1.504	1.554	88.33

[a] X denotes F or Cl; bond distances in angstroms, angles in degrees. [b] X1 denotes the halogen of the neutral molecule. [c] X2 denotes the nucleophilic halogen. [d] I_{RC} denotes stable prepentacoordinate intermediate. [e] I_{TS} denotes transition state. [f] I_{PC} denotes stable postpentacoordinate intermediate.

TABLE 6: Overall Activation Energies ($E^{\#}_{over}$), Central Activation Energies ($E^{\#}_{cent}$), and Complexation Energy (E_{comp}) Calculated at the CCSD(T)/aug-cc-pVTZ Level of Theory[a]

	$E^{\#}_{over}$(R)	$E^{\#}_{over}$(I)	$E^{\#}_{cent}$(R)	$E^{\#}_{cent}$(I)	E_{comp}(R)	E_{comp}(I)
Cl^- + CH_3Cl	46.69	1.23	57.54	12.08	−10.85	−10.85
	(46.32)[b]	(1.96)[c]	(56.84)[b]			(−10.48)[c]
F^- + CH_3F	44.45	−1.26	58.46	12.75	−14.01	−14.01
	(44.10)[b]	(−1.11)[d]	(57.60)[b]			(−14.15)[d]
Cl^- + SiH_3Cl	−7.47	−26.35	3.85		−11.32	
		(−27.11)[c]				
F^- + SiH_3F	−46.18	−54.51	2.09		−48.27	

[a] R and I stand for the reactions with retention and inversion of configuration, respectively; energies in kilocalories per mole. [b] Values (in parentheses) calculated at the G2 (+) level.[11] The over barrier, $E^{\#}_{over}$, our computational value (2.02 eV) agrees well with the experimental estimate of the overall barrier for Cl^- + CH_3Cl at higher energies (2.0 eV).[9] [c] Values (in parentheses) calculated at the CCSD(T)/aug-cc-pVTZ level.[6] [d] Values (in parentheses) calculated at the CCSD(T)/aug-cc-pVTZ level.[5]

repulsion to the negatively charged $X2^-$ (nucleophile). This electrostatic effect is so large that the front-side attack pathways are hindered for the $S_N2(C)$ and $S_N2(Si)$ reactions.

Of course, the energy profile along the IRC route that contains both the steric and electrostatic effects can decide which one is preferred (retention or inversion pathway). As discussed above, for the $S_N2(C)$ reactions with Cl^- and F^-, the activation energies of inversion pathways are much lower than those of corresponding retention pathways. (See Table 6.) Therefore, $S_N2(C)$ reactions prefer to proceed via inversion pathways. For the $S_N2(Si)$ reactions with Cl^-, its activation energy of the inversion pathway is also much lower than that of the corresponding retention pathway, so it is inclined to an inversion pathway over a retention pathway. And the difference between activation energies of retention and inversion pathways is relatively smaller for the $S_N2(Si)$ reactions with F^-, so retention and inversion pathways compete for the course of the reaction in the gas phase.

3.2. Analysis of Potential Acting on an Electron in a Molecule for $S_N2(C)$ and $S_N2(Si)$ Reactions with Retention of Configuration. ***3.2.1. Pictures of Potential Acting on an Electron in a Molecule among Nucleophile, Central Atom, and Leaving Group along the Intrinsic Reaction Coordinate Route.*** The definition of the potential acting on electron in a molecule (PAEM) has been described in Section 2.2. On the basis of the PAEM theory, the D_{pb} for a chemical bond has been recently defined by Yang and coworkers.[38] It is a new

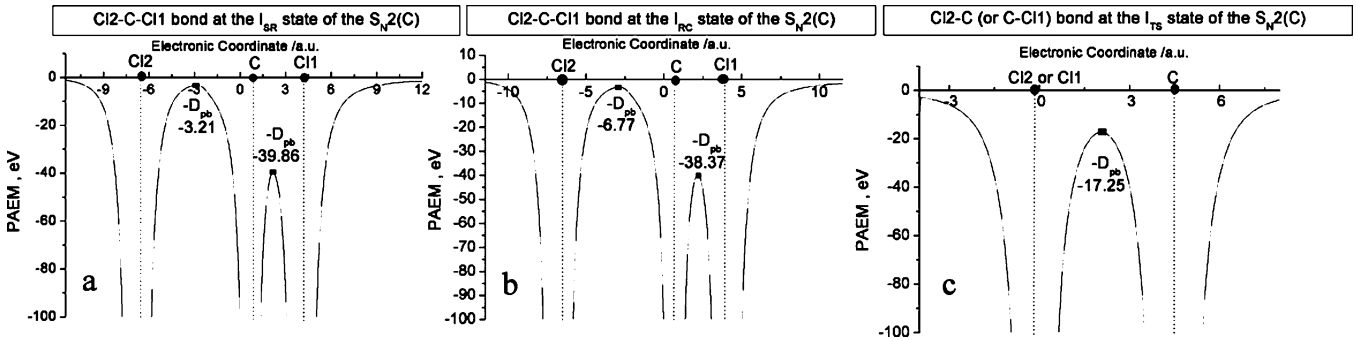

Figure 4. Pictures of PAEM among nucleophile, central atom, and leaving group for the $S_N2(C)$ reaction with Cl^- at (a) I_{SR}, (b) I_{RC}, and (c) I_{TS} states along IRC routes.

TABLE 7: D_{pb} of C−Cl1 and C−Cl2 Bonds for the Front-Side Attack $S_N2(C)$ Reaction with Cl^- along the IRC Route[a]

	state	I_{SR}[b]	I_{RC}[c]	I_{TS}[d]	I_{PC}[e]
D_{pb}	C−Cl1	39.86	38.37	17.25	6.77
	C−Cl2	3.21	6.77	17.25	38.37

[a] D_{pb} in eV. [b] Geometry of the I_{SR} state is fully optimized in C_{3v} symmetry by constraining the Cl2−C distance (3.95 Å) for $[CH_3Cl_2]^-$ molecular system. [c] I_{RC} denotes pre-ion-complex. [d] I_{TS} denotes transition state. [e] I_{PC} denotes post-ion-complex.

physical quantity for representing the strength of a chemical bond. The D_{pb} is the energy gap from the saddle point of the PAEM along a chemical bond axis to the zero level of energy and characterizes how easily the electron moves from one nuclear region to another nuclear region through the bond region, in other words, how high a PAEM barrier the electron should overcome from one nuclear region to the other nuclear region through the bond region. The characteristic features of the PAEMs in the bond regions are depicted in Figure 4 along the IRC route for the $S_N2(C)$ reaction with Cl^-, where the horizontal axis denotes the electron coordinate along the bond axis, and the vertical axis denotes the PAEM. The corresponding computational D_{pb} values are listed in Table 7. It can be seen that the common character of the PAEMs is that they gently vary in the farther nuclear region and decrease sharply around a nuclear region that just likes a lake that accommodates electrons. The bigger the nuclear charge is, the wider the potential is. The PAEM between two nuclei has a potential saddle point that corresponds to minus of D_{pb} and indicates whether the electron flows easily while passing through this saddle.

Now we present the pictures of the PAEMs among nucleophile, central atom, and leaving group along the IRC route. The reaction $CH_3Cl1 + Cl2^- \rightarrow CH_3Cl2 + Cl1^-$ is taken for an illustrative example; the pictures for the other reactions are analogous, so the calculated results are given in the Supporting Information (Table S9). Four points (I_{SR}, I_{RC}, I_{TS}, I_{PC}) are picked out along the IRC route. Here the geometry of I_{SR} is fully optimized in C_{3v} symmetry by constraining the Cl2−C distance (3.950 Å), I_{RC} denotes pre-ion-complex, I_{TS} denotes transition state, and I_{PC} denotes post-ion-complex. When the distance between $Cl2^-$ and C is very large, the electron between them feels very high potential energy; that is, the electron between $Cl2^-$ and CH_3Cl1 is restrained around their respective nuclear regions and is rarely capable of flowing between them. In other words, the electron dominantly moves in the classical forbidden region. At the I_{SR} state, the D_{pb} of the C−Cl2 "bond" is 3.21 eV, which is smaller than the ionization potential (3.79 eV) of this state, indicating that the electron between $Cl2^-$ and CH_3Cl1 still mainly moves in the classical forbidden region and does not flow classically. However, the D_{pb} of the C−Cl1 bond is 39.86 eV, which is much larger than the ionization potential of this state, as if the electron between Cl1 and C flows in the deeper channel between the two atomic electron lake, indicating that the C−Cl1 bond is a strong bond. When the $Cl2^-$ gradually attacks C and the pre-ion−molecule complex forms, the D_{pb} of the C−Cl2 "bond" increases to 6.77 eV, and the D_{pb} of the C−Cl1 bond decreases a little to 38.37 eV, but both are larger than the ionization potential (3.98 eV) of this state, indicating that the electron can commutatively flow between not only C and Cl1 but also C and Cl2. However, the capacity of forming a bond between C and Cl2 is very weak compared with that between C and Cl1. When $Cl2^-$ further attacks C, namely, at the reaction transition state, the D_{pb} values of C−Cl2 and C−Cl1 bonds both become 17.25 eV. The comparison with the above-stated I_{RC} state shows that the former increases by 10.48 eV, and the latter decreases by 21.12 eV. This indicates that the C−Cl2 bond becomes stronger, but the C−Cl1 bond becomes weaker, although they are identical at this state. After the TS state, $Cl2^-$ further approaches C; namely, Cl1 (leaving group) gradually goes away from C. This is only the mirror image process from reactants to TS, so we do not describe it in detail.

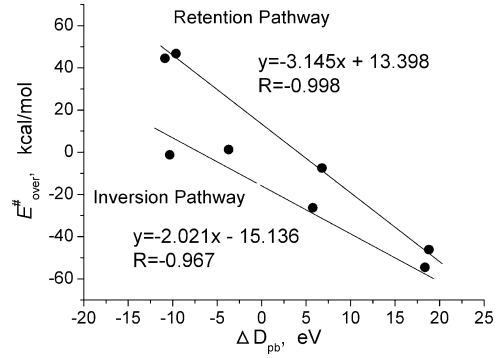

Figure 5. Correlation between the difference of D_{pb} of the separate reactant and TS or TC (ΔD_{pb}) and the overall activation barriers ($E^{\#}_{over}$) for the front-side and back-side attacks identity $S_N2(C)$ and $S_N2(Si)$ reactions with Cl^- and F^-.

3.2.2. Analysis of D_{pb} for Front-Side and Back-Side Attacks Identity $S_N2(C)$ and $S_N2(Si)$ Reactions. First, we find a correlation between the difference of the D_{pb} of the separate reactant and TS (TC) (denoted by ΔD_{pb}) and overall activation barriers ($E^{\#}_{over}$) for the front-side and back-side attacks identity $S_N2(C)$ and $S_N2(Si)$ reactions. Their linear correlations are drawn in Figure 5, and the D_{pb} values of reactants and TSs (TCs) are given in Table 8. There are good linear correlations between ΔD_{pb} and $E^{\#}_{over}$ for both $S_N2(C)$ and $S_N2(Si)$ reactions with retention and inversion of configuration, and their correlation coefficients are −0.998 and −0.967, respectively. Note that

TABLE 8: D_{pb} of C−H, C−Cl, C−F, Si−H, Si−Cl, and Si−F Bonds for the Reactants and TSs (TCs)[a]

	D_{pb}					
	C−H bond			C−X bond		
system	I_{REA}[b]	I_{TS}(R)	I_{TS}(I)	I_{REA}	I_{TS}(R)	I_{TS}(I)
$Cl^- + CH_3Cl$	49.26	48.83	49.61	43.69	17.25	19.81
$F^- + CH_3F$	52.04	45.74	48.15	56.12	25.78	24.84
	Si−H bond			Si−X bond		
system	I_{REA}[b]	I_{TS}(R)	I_{TS}(I)	I_{REA}	I_{TS}(R)	I_{TS}(I)
$Cl^- + SiH_3Cl$	41.54	32.96	36.69	42.07	28.72	26.34
$F^- + SiH_3F$	41.23	31.47	36.62	53.73	41.15	38.35

[a] X denotes F or Cl; R and I stand for the reactions with retention and inversion of configuration, respectively; D_{pb} in electronvolts. [b] I_{REA} denotes separate reactant.

ΔD_{pb} is an inverse measure of $E^{\#}_{over}$. This is easily understood in terms of our model. D_{pb} is a positive quantity (Figure 4), and the larger D_{pb} is, the stronger the bond is. Therefore, the larger positive ΔD_{pb} corresponds to the lower activation energy for the course of the reactions. It is necessary to explain that in our studies, the ΔD_{pb} between nucleophile and central atom in the initial state is regarded to be zero.

Next, we analyze the pictures of average values of the D_{pb} for C−H and Si−H bonds of the front-side and back-side attack S_N2(C) and S_N2(Si) reactions along IRC routes. The changing curves of D_{pb} and the potential energy profiles of these reactions are drawn in Figure 6, and the corresponding calculated results are given in the Supporting Information (Table S10). Here I_{SR1} and I_{SR2} are the two states, and their geometries are fully optimized in C_{3v} symmetry by constraining the distance between the nucleophile and central atom (3.950 and 3.500 Å for I_{SR1} and I_{SR2}, respectively). Interestingly, a comparison of Figure 6a and a′ indicates that the changing trends of D_{pb} and relative energies are very similar. We have analyzed the calculated results and Figure 6 carefully and then observed that the D_{pb} values of the C−H bonds of both back-side attack S_N2(C)

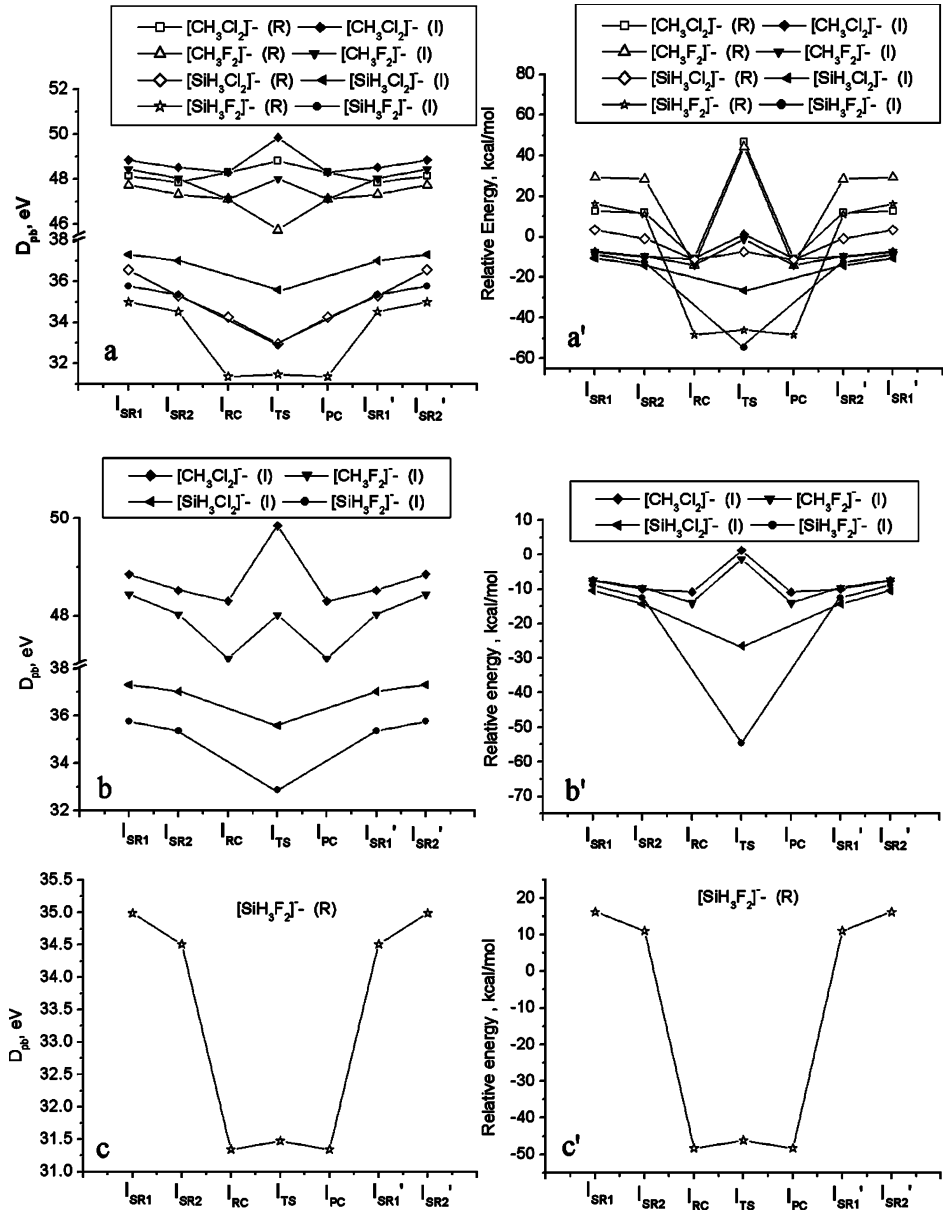

Figure 6. Curves of D_{pb} and the potential energy profiles for the S_N2(C) and S_N2(Si) reactions with retention and inversion of configuration along the IRC routes.

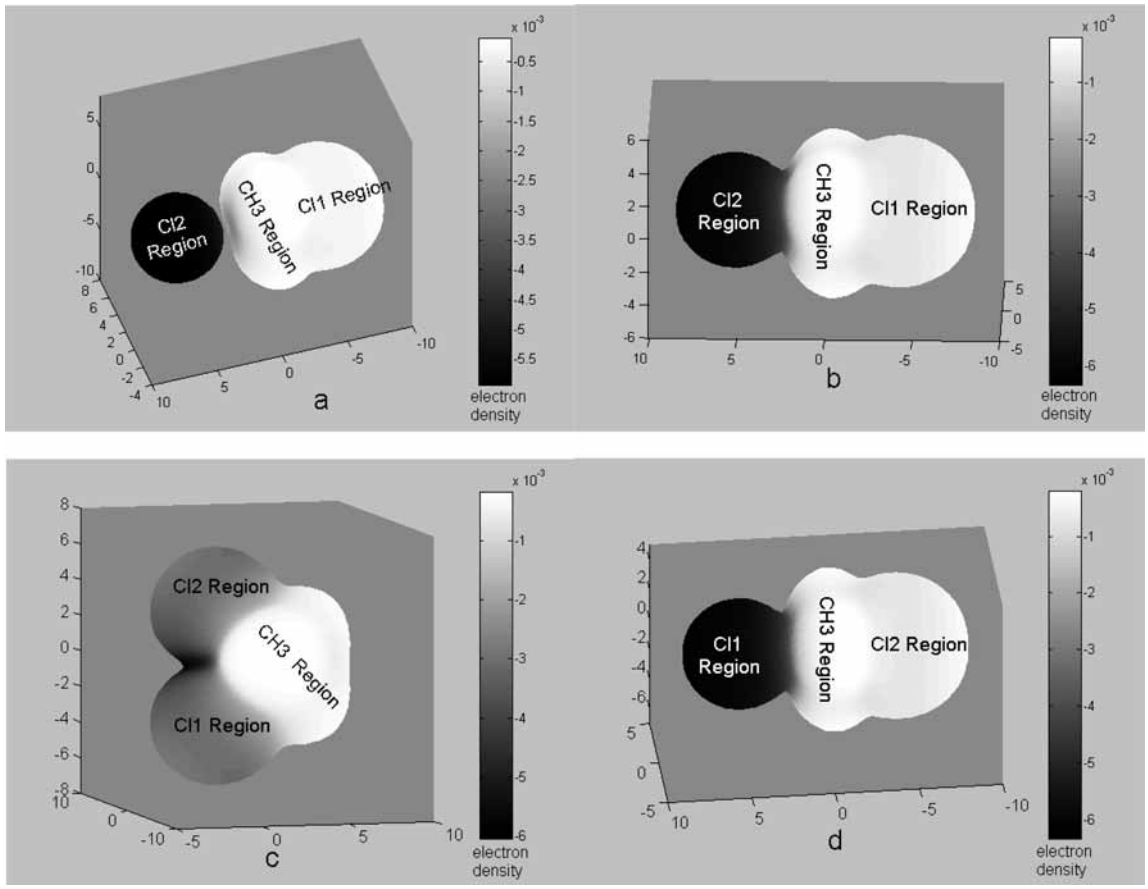

Figure 7. Spatial dynamic changing features of the MFs for the front-side attack identity $S_N2(C)$ reaction with Cl^- along the IRC route: (a) I_{SR}, (b) I_{RC}, (c) I_{TS}, and (d) I_{PC}. The magnitude of electron density on a MF is in proportion to the surface gray scale, where darker areas denote larger density and brighter areas denote smaller density. The vivid color MF features corresponding to these white and black ones are included in the Supporting Information (Figure S4).

TABLE 9: Molecular Intrinsic Characteristic Parameters Obtained by the MF Model[a]

system		R_{out}^{X1}	R_V^{X1}	R_{out}^{X2}	R_V^{X2}	ED_{out}^{X1}	ED_V^{X1}	ED_{out}^{X2}	ED_V^{X2}
$[CH_3Cl_2]^-$(R)	I_{SR}	4.75	4.68	3.29	3.30	0.12	0.34	5.82	5.82
	I_{RC}	4.40	4.33	3.26	3.29	0.28	0.74	6.30	5.93
	I_{TS}	3.64	3.56	3.64	3.56	3.00	3.25	3.00	3.25
	I_{PC}	3.26	3.29	4.40	4.33	6.30	5.93	0.28	0.74

[a] Distance in a.u., electron density in $\times 10^{-3}$ a.u., and X denotes F or Cl.

reactions with F^- and Cl^- show a double-well energy profile along the IRC routes, and D_{pb} values of the Si−H bonds of the back-side attack $S_N2(Si)$ reactions show a single-well energy profile along the IRC routes, which are similar to their respective double-well and single-well energy profiles obtained at the CCSD(T)/aug-cc-pVTZ level of theory. (See Figure 6b,b′.) For the front-side attack identity $S_N2(Si)$ reactions with F^-, the D_{pb} values of Si−H bonds show a double-well energy profile along the IRC route perfectly, which is very similar to its double-well energy profile (Figure 6c,c′).

3.3. Studies of the Molecular Face for $S_N2(C)$ and $S_N2(Si)$ Reactions with Retention of Configuration. ***3.3.1. Description of the Spatial Dynamic Changing Features of Molecular Face along Intrinisic Reaction Coordinate Route.*** The spatial dynamic changing features of MFs are depicted for the course of the S_N2 reactions. The visualized MFs are presented in Figure 7a−d for $[CH_3Cl_2]^-$. The magnitude of electron density on a MF is in proportion to the surface gray scale, where darker areas denote larger density and brighter areas denote smaller density. In this section, $CH_3Cl1 + Cl2^- \rightarrow CH_3Cl2 + Cl1^-$ is still taken for an illustrative example; the other reactions are analogous, so the calculated results are given in the Supporting Information (Table S11 and Figures S1−S3). To describe the interaction between halide anion and halomethane or halosilane in more detail, it is necessary to define several parameters. On the horizontal molecular plane including atoms Cl2, C, and Cl1, a straight line passing through nuclei Cl2 and C has two intersection points with the molecular MF contour, so R_{out}^{Cl2} and R_{in}^{Cl2} are the distances from the Cl2 nucleus outwards and inwards to the intersection point on the MF of Cl2, and the corresponding electron densities on those points are denoted by ED_{out}^{Cl2} and ED_{in}^{Cl2}, respectively. On the vertical molecular plane, a straight line passing through Cl2 nucleus and vertical to the C−Cl2 internuclear axis has two intersection points with the MF of Cl2, and hence the distance from the Cl2 nucleus to the intersection point is denoted by R_v^{Cl2}, and the corresponding electron density is written as ED_v^{Cl2}. The other molecular intrinsic characteristic parameters have similar definition, and the calculated results of $S_N2(C)$ with Cl^- for the states interested are listed in Table 9.

At the I_{SR} state, the contours of Cl2 and CH_3Cl1 remain separated, as shown in Figure 7a. Looking at this picture, the

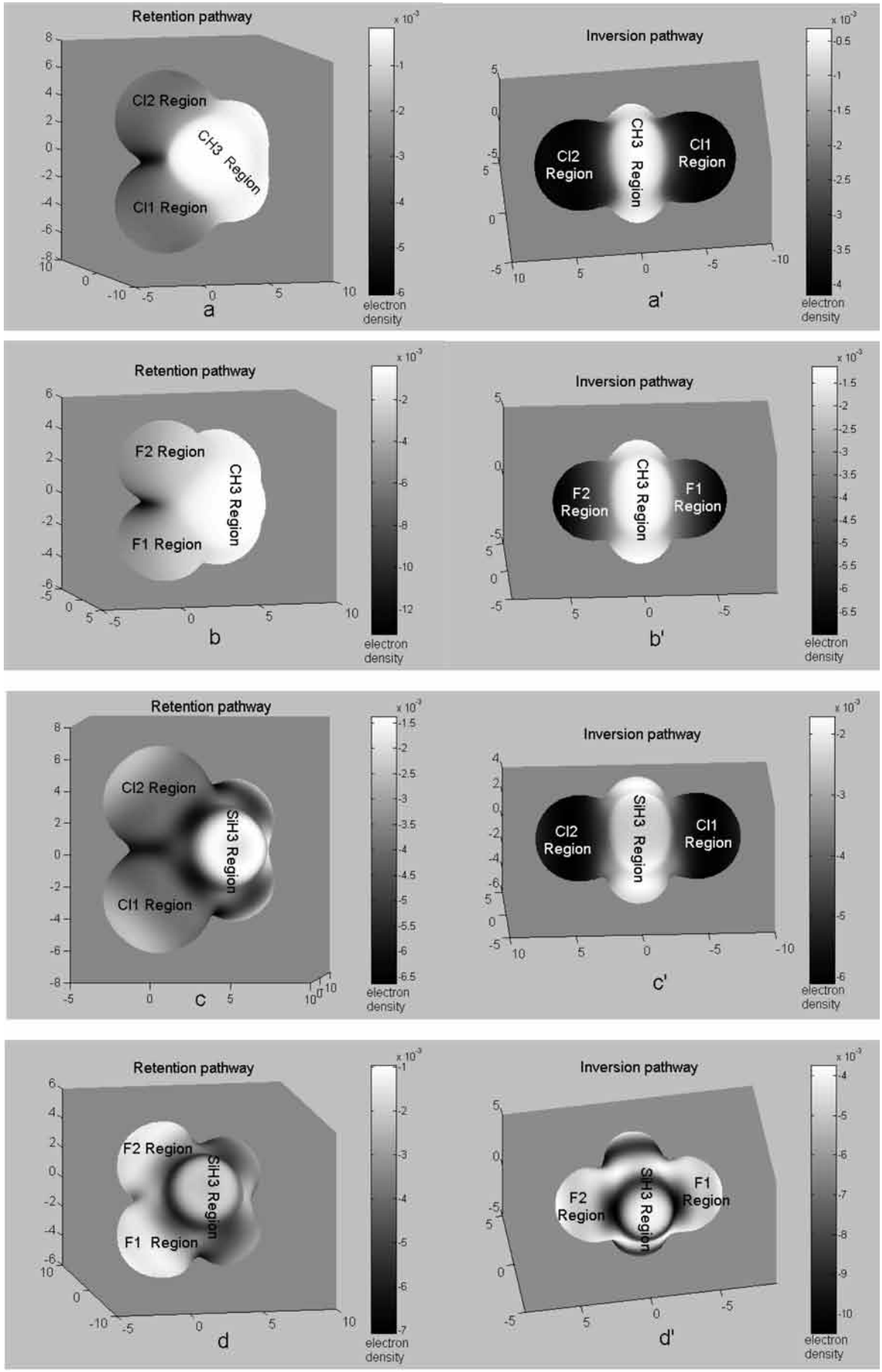

Figure 8. Features of MF of TSs (TCs) for the $S_N2(C)$ and $S_N2(Si)$ reactions with retention and inversion of configuration. The vivid color MF features corresponding to these white and black ones are included in the Supporting Information (Figure S5).

first striking impression to our eyes is that the color of the Cl2 region is much darker than that of the Cl1 region, meaning that the electron density of the Cl2 region is much larger than that of the Cl1 region. Another interesting phenomenon is that the interaction causes the contours to expand toward each other. For Cl2, R_{in}^{Cl2} (3.49 a.u.) is larger than R_{out}^{Cl2} by 0.20 a.u., indicating that the interpolarization effect arises between Cl2 and CH_3Cl1. But here R_{out}^{Cl2} and R_V^{Cl2} are much smaller than R_{out}^{Cl1} and R_V^{Cl1} (Table 9), respectively. When the pre-ion-complex is formed, on one hand, ED_{out}^{Cl2} and ED_V^{Cl2} are much larger than ED_{out}^{Cl1} and ED_V^{Cl1}, respectively, indicating that the most negative charges concentrate on the Cl2 region. On the other hand, the contour of Cl2 is still much smaller than that of Cl1; R_{out}^{Cl2} and R_v^{Cl2} are only 3.26 and 3.29 a.u, respectively, but R_{out}^{Cl1} and R_v^{Cl1} are 4.40 and 4.33 a.u. respectively. At the transition state, the electron density is symmetrical distribution in both sides of the C_s symmetry plane. The comparison with the I_{SR} state shows that ED_{out}^{Cl2} suddenly becomes smaller, but ED_{out}^{Cl1} becomes larger. This indicates that the electron transfers from Cl2 to Cl1. Another remarkable feature is that the contour of Cl2 gradually becomes large, and the contour of Cl1 gradually becomes small, and as a result, the former and the latter become identical. When Cl2 further approaches C, namely, Cl1 gradually goes away from C; this is only the mirror image process from I_{SR} state to TS.

3.3.2. Analysis of Molecular Face of the Transition States for Front-Side Attack Identity S_N2(C) and S_N2(Si) Reactions Compared with Corresponding Back-Side Attack Ones. In this section, we compare the descriptions of MFs for TSs (TCs) for the front-side attack S_N2(C) and S_N2(Si) reactions with those of back-side attack ones. Their features of MFs are depicted in Figure 8, and the calculated molecular intrinsic characteristic parameters are given in Table 9 and in the Supporting Information (Tables S11 and S12). Several observations can be obtained from the calculated results and Figure 8. Looking at Figure 8, the first striking impression is that electron density of Cl and F atom regions of back-side attack identity S_N2(C) and S_N2(Si) reactions is obviously larger than that of corresponding front-side attack ones, except for S_N2(Si) reaction with F^-. This indicates that the partial negative charges concentrate on the two sides of Cl and F atom regions for inversion pathways. A comparison of front-side attack identity S_N2(Si) reactions with S_N2(C) reactions shows that the partial negative charges concentrate more on the connected regions between the SiH_3 group and the halogen atom than that between CH_3 group and halogen atom. Another interesting feature is that the contours of Cl and F atoms of the front-side attack identity S_N2(C) and S_N2(Si) reactions are larger than those of corresponding back-side attack ones.

4. Conclusions

In this article, we have studied the gas-phase front-side attack identity S_N2(C) and S_N2(Si) reactions with F^- and Cl^- by the ab initio method and MF theory compared with the corresponding back-side attack ones. A front-side attack identity S_N2(Si) reaction with F^- or Cl^- has a double-well PES. The reactants initially form a stable pentacoordinated anion intermediate of C_s symmetry (TBP), then pass through a C_s transition state (SP) to a complementary pentacoordinated intermediate (TBP), and finally dissociate into separate products. Berry pseudorotation of the S_N2(Si) reactions has been observed via the ab initio study, which has supported the conclusion proposed by Holmes et al.

In terms of the MF theory, we have demonstrated some features of these reactions. The difference in D_{pb} between reactant and TS (TC) can be related to the activation energy of the S_N2 reactions. The D_{pb} curves of these reactions have a double-well energy profile or a single-well energy profile along the IRC routes, which are similar to their respective double-well or single-well potential energy profiles obtained at the CCSD(T)/aug-cc-pVTZ level of theory. Furthermore, the interesting pictures of formation or rupture of the chemical bond and the spatial dynamic changing features of the molecular shapes and the face electron density are vividly depicted by the MF theory for the course of the reactions.

In addition, for the gas-phase front-side attack identity S_N2(C) and S_N2(Si) reactions, their initial attacks and transition-state positions are completely different, and their electron density distribution on MF and shape of the contours for the TSs are also different, but the main difference between them is that S_N2(Si) reactions proceed via Berry pseudorotation in the course of the reactions, whereas S_N2(C) reactions do not proceed. But they undergo similar three-center transition states, which are isoelectronic in view of valence electrons and isostructural in view of the geometric types of the main species along the IRC routes.

Acknowledgment. This research is supported by the National Science Foundation of China (grant nos. 20633050 and 20703022 and LNET project no. RC0503), 2007T091 and 2008S133 from Educational Department of Liaoning Province. We thank Prof. E. R. Davidson for providing us with the MELD package and other kind help. We acknowledge the valuable suggestions from the Editor Prof. Xueming Yang and the reviewers.

Supporting Information Available: The geometries of species involved in the S_N2 reactions, MP2 activation energies, energies of reactants, complexes (intermediates) and TSs (TCs), the calculated molecular intrinsic characteristic parameters and D_{pb}, the features of MF for the S_N2 (C) and S_N2(Si) reactions, and vivid color MF features corresponding to the white and black ones of Figures 7 and 8. This material is available free of charge via the Internet at http://pubs.acs.org.

References and Notes

(1) Ingold, C. K. *Structure and Mechanism in Organic Chemistry*; Cornell University Press: Ithaca, NY, 1969.
(2) March, J. *Advanced Organic Chemistry: Reactions, Mechanisms, and Structure*, 4th ed.; Wiley-Interscience: New York, 1992
(3) Mo, Y. R.; Gao, J. L. *J. Comput. Chem.* **2000**, *21*, 1458.
(4) Vayner, G.; Houk, K. N.; Jorgensen, W. L.; Brauman, J. I. *J. Am. Chem. Soc.* **2004**, *126*, 9054.
(5) Gonzales, J. M.; Allen, W. D.; Schaefer, H. F., III *J. Phys. Chem. A* **2005**, *109*, 10613.
(6) Bento, A. P.; SolÀ, M.; Bickelhaupt, F. M. *J. Comput. Chem.* **2005**, *26*, 1497.
(7) Pierrefixe, S. C. A. H.; Cuerra, C. F.; Bickelhaupt, F. M. *Chem.—Eur. J.* **2008**, *14*, 918.
(8) ELGomati, T.; Lenoir, D.; Ugi, I. *Angew. Chem., Int. Ed. Engl.* **1975**, *14*, 59.
(9) Barlow, S. E.; Doren, J. M. V.; Bierbaum, V. M. *J. Am. Chem. Soc.* **1988**, *110*, 7240.
(10) Deng, L.; Branchadell, V.; Ziegler, T. *J. Am. Chem. Soc.* **1994**, *116*, 10645.
(11) Glukhovtsev, M. N.; Pross, A.; Radom, L. *J. Am. Chem. Soc.* **1995**, *117*, 2024.
(12) Glukhovtsev, M. N.; Pross, A.; Schlegel, H. B.; Bach, R. D.; Radom, L. *J. Am. Chem. Soc.* **1996**, *118*, 11258.
(13) Li, G.; Hase, W. L. *J. Am. Chem. Soc.* **1999**, *121*, 7124.
(14) Holmes, R. R. *Five-Coordinated Struxrogress in Inorganic Chemistry*; Lippard, S. J., Ed.; Wiley: New York, 1984; Vol. 32, pp 119−235.
(15) Holmes, R. R.; Day, R. O.; Harland, J. J.; Sau, A. C.; Holmes, J. M. *Organometallics* **1984**, *3*, 341.
(16) Holmes, R. R.; Day, R. O.; Harland, J. J.; Holmes, J. M. *Organometallics* **1984**, *3*, 347.

(17) Holmes, R. R.; Day, R. O.; Chandrasekhar, V.; Holmes, J. M. *Inorg. Chem.* **1985**, *24*, 2009.
(18) Holmes, R. R.; Day, R. O.; Chandrasekhar, V.; Harland, J. J.; Holmes, J. M. *Inorg. Chem.* **1985**, *24*, 2016.
(19) Corriu, R. J. P.; Kpoton, A.; Poirier, M.; Royo, G.; Corey, J. Y. *J. Organomet. Chem.* **1984**, *277*, C25.
(20) Keil, F.; Ahlrichs, R. *J. Am. Chem. Soc.* **1976**, *98*, 4787.
(21) Deiters, J. A.; Holmes, R. R. *J. Am. Chem. Soc.* **1987**, *109*, 1686.
(22) Deiters, J. A.; Holmes, R. R. *J. Am. Chem. Soc.* **1987**, *109*, 1692.
(23) Deiters, J. A.; Holmes, R. R.; Holmes, J. M. *J. Am. Chem. Soc.* **1988**, *110*, 7672.
(24) Gronert, S.; Glaser, R.; Streitwieser, A. *J. Am. Chem. Soc.* **1989**, *111*, 3111.
(25) Windus, T. L.; Gordon, M. S.; Davis, L. P.; Burggraf, L. W. *J. Am. Chem. Soc.* **1994**, *116*, 3568.
(26) Bento, A. P.; Bickelhqupt, F. M. *J. Org. Chem.* **2007**, *72*, 2201.
(27) Holmes, R. R. *Pentacoordinated Phosphorus: Reaction Mechanisms*; ACS Monograph No. 176; American Chemical Society: Washington, DC, 1980; Vol. II.
(28) Westheimer, F. H. *Acc. Chem. Res.* **1968**, *1*, 70.
(29) Berry, R. S. *J. Chem. Phys.* **1960**, *32*, 933.
(30) Corriu, R. J. P.; Guerin, C. *J. Organomet. Chem.* **1980**, *198*, 231.
(31) Yang, Z. Z.; Davidson, E. R. *Int. J. Quantum Chem.* **1996**, *62*, 47.
(32) Yang, Z. Z.; Zhao, D. X. *Chem. Phys. Lett.* **1998**, *292*, 387.
(33) Zhao, D. X.; Yang, Z. Z. *THEOCHEM* **2002**, *579*, 73.
(34) Yang, Z. Z.; Zhao, D. X.; Wu, Y. *J. Chem. Phys.* **2004**, *121*, 3452.
(35) Gong, L. D.; Zhao, D. X.; Yang, Z. Z. *THEOCHEM* **2003**, *636*, 57.
(36) Yang, Z. Z.; Gong, L. D.; Zhao, D. X.; Zhang, M. B. *J. Comput. Chem.* **2005**, *26*, 35.
(37) Zhang, M. B.; Yang, Z. Z. *J. Phys. Chem. A* **2005**, *109*, 4816.
(38) Zhao, D. X.; Gong, L. D.; Yang, Z. Z. *J. Phys. Chem. A* **2005**, *109*, 10121.
(39) Yang, Z. Z.; Ding, Y. L.; Zhao, D. X. *ChemPhysChem* **2008**, *9*, 2379.
(40) Zhao, D. X.; Yang, Z. Z. *J. Theor. Comput. Chem.* **2008**, *7*, 303.
(41) Purvis, G. D.; Bartlett, R. J. *J. Chem. Phys.* **1982**, *76*, 1910.
(42) Woon, D. E.; Dunning, T. H., Jr. *J. Chem. Phys* **1993**, *98*, 1358.
(43) Møller, C.; Plesset, M. S. *Phys. Rev.* **1934**, *46*, 618.
(44) Hehre, W. J.; Radom, L.; Schleyer, P. v. R.; Pople, J. A. *Ab initio Molecular Orbital Theory*; Wiley: New York, 1986.
(45) Fukui, K. *Acc. Chem. Res.* **1981**, *14*, 363.
(46) Davidson, E. R. MELD Program Description. In *MOTECC*; ESCOM: New York, 1990, 553.
(47) Harmony, M. D.; Laurie, V. W.; Kuczkowski, R. L.; Schwendeman, R. H.; Ramsay, D. A.; Lovas, F. J.; Lafferty, W. J.; Maki, A. G. *J. Phys. Chem. Ref. Data* **1979**, *8*, 619.
(48) *CRC Handbook of Chemistry and Physics*, 84th ed.; Lide, D. R., Ed.; CRC Press: Boca Raton, FL, 2003.

JP804951W